Numerical modelling of hydrodynamics of permeable pile groins using SWASH

Zhang, Rong; Stive, Marcel

DOI
10.1016/j.coastaleng.2019.103558

Publication date
2019

Document Version
Final published version

Published in
Coastal Engineering

Citation (APA)
Zhang, R., & Stive, M. (2019). Numerical modelling of hydrodynamics of permeable pile groins using SWASH. *Coastal Engineering*, *153*, Article 103558. https://doi.org/10.1016/j.coastaleng.2019.103558

Coastal Engineering 153 (2019) 103558

Contents lists available at ScienceDirect

Coastal Engineering

journal homepage: http://www.elsevier.com/locate/coastaleng

Numerical modelling of hydrodynamics of permeable pile groins using SWASH

Rong Zhang *, Marcel J.F. Stive

Department of Hydraulic Engineering, Delft University of Technology, Delft, the Netherlands

ARTICLE INFO

Keywords:
Longshore currents
SWASH
Numerical modelling
Pile groins

ABSTRACT

This paper focuses on a specific form of groins, Permeable Pile Groins (PPGs), consisting of a single or double rows of wooden piles. With only few experiments and simulations available to study the hydraulic functioning of PPGs, the correlation between the effectiveness and the characteristics of the groin system has yet to be fully understood. This paper presents the application of SWASH, a non-hydrostatic wave-flow model to simulate flow fields affected by PPGs. The SWASH model was calibrated to correctly reproduce longshore current fields in the laboratory. Then, introducing PPGs in the model, the simulation results are compared with available experimental measurements to investigate current-PPG interaction. The simulation results, which generally agree well with the measurements, show that PPGs hardly attenuate wave energy but considerably retard longshore currents within the groin fields. Rip currents are predicted to develop at both flank sides of each pile groin, due to local positive water level gradients toward the pile groins.

1. Introduction

Coastal groins (or groynes), generally constructed perpendicular to the shore, are one of the most popular coastal protection structures. Groins contribute to the build-up of coasts and the widening of beaches via a) producing a sheltered area at the leeside of a groin due to wave diffraction; b) hindering wave induced longshore currents; c) deflecting strong tidal currents; d) intercepting longshore sediment transport (Bakker et al., 1970). Considering the aspect of permeability, groins could be divided into permeable groins and impermeable groins. Impermeable groins are solid groins made of concrete, stone, wood or steel, which block the flow cells in groin fields. Permeable groins, made of wooden piles or porous stone or concrete modules, allow flow to pass through. The distinct advantage of permeable groins compared with impermeable groins is that permeable groins allow a fraction of the longshore sediment transport passing through their openings. A decrease in the blockage ratio of longshore sediment transport could alleviate the sand starvation of the coast downdrift permeable groins, where commonly large scale erosion occurs in the presence of impermeable groins. Moreover, unlike the commonly discontinuous shoreline interrupted by impermeable groins, the shoreline response to permeable groins is continuous (Bakker et al., 1984; Raudkivi, 1996; Trampenau et al., 1996). For instance, a continous nearly stranght shoreline response to a permeable groin system is shown in Fig. 1. In this paper, only one specific form of permeable groins, permeable pile groins (PPGs) consisting of wooden piles, was considered. Due to the appealing natural look, the ease of construction and the usage of renewable timber resources, PPGs attract more attention in coastal engineering projects especially from an environmental concern (Perdok, 2002; Crossman and Simm, 2002). PPGs have been widely utilised to protect coasts from erosion in Europe, for instance, at the North Sea coasts in the Netherlands and the United Kingdom (Price et al., 1972; Bakker et al., 1984), and the Baltic Sea coasts in Germany and Poland (Raudkivi, 1996; Trampenau et al., 1996; Raudkivi and Dette, 2002; Dette et al., 2004; Strusiańska-Correia, 2014).

The functional mechanism of permeable pile groins, as concluded by Raudkivi (1996), is that PPGs act as hydraulic resistances to slow down longshore currents. The reduction of littoral current velocity leads to less turbulence produced by the wave-current interaction at the bed. Consequently, fewer sediment particles are mobilized. Therefore, the retarded longshore currents transport a reduced amount of sediment. As a result, the sediment is easily trapped and retained in the vicinity of the groins. The pile groins do not alter the characteristics of incident waves, which are negligible considering the wide spacing between each PPG alongshore (Raudkivi, 1996), except for a very limited wave shadow area near each PPG.

* Corresponding author.
E-mail address: R.Zhang@tudelft.nl (R. Zhang).

https://doi.org/10.1016/j.coastaleng.2019.103558
Received 29 August 2018; Received in revised form 17 July 2019; Accepted 13 September 2019
Available online 18 September 2019

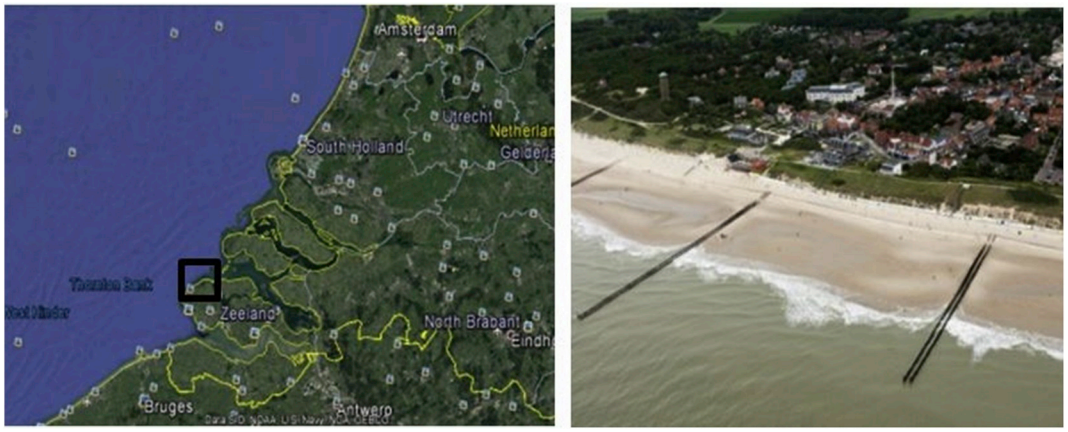

Fig. 1. Left: The location of a pile groin engineered coast in Zeeland Province, The Netherlands (in the black rectangle, from Google earth); right: the continuous straight shoreline response to PPGs at the coast (source: https://beeldbank.rws.nl, Rijkswaterstaat).

Field surveys showed that the coastline recession was effectively curbed and the nearshore accretion was promoted by massive rows of pile groins (Kolp, 1970; Price et al., 1972; Trampenau et al., 2004; Abam, 2009). To further investigate the effects of pile groins on nearshore currents, a laboratory experiment under exquisitely controlled conditions is another effective method. When the average permeability of a pile groin is 55%, Hulsbergen and ter Horst, 1973 measured a 40% reduction of longshore current velocities within groin fields, under a combined wave and steady current condition. For the case of obliquely incident monochromatic waves in the experiment conducted by Trampenau et al., 2004, the purely wave-induced longshore current reduced to 40% of the undisturbed longshore current velocities, in the fields of groins with a 30% permeability, and to 70% in the fields of groins with a 50% permeability. Uijttewaal (2005) compared the turbulence properties near and downstream of permeable and solid groins. This author concluded that for permeable pile groins, the shear and turbulence intensity can be significantly reduced at the mixing layer between the groin fields and the main stream, and the rather unidirectional flow passing through permeable groins prevented the formation of a recirculation flow in groin fields, in contrast to solid groins.

Field studies and laboratory experiments proved that, to a large extent, PPGs slow down longshore currents and effectively curb coastline recession. In addition, timber PPGs are considered kind of appealing structures, especially at recreational coasts with a high aesthetic appreciation. The reason is that the small footprints of PPGs harm beach amenity to a small extent, and the renewable wooden construction material is environmentally friendly and economically (Perdok et al., 2003; Crossman, 2004, e.g. PPGs at a beach resort in Zeeland province, The Netherlands, Fig. 1). However, an important consideration of beach erosion is that possible strong rip currents, incited by the existence of groins, could lead to seaward loss of beach material (Bakker et al., 1984).

Although for centuries PPGs have been applied in coastal engineering, relatively few detailed and high resolution measurements are available either from field studies or laboratory researches. To bridge the gap, numerical simulations are employed to study nearshore flow within permeable groin fields. The representative data sets obtained from the laboratory experiments (Hulsbergen and ter Horst, 1973) are selected to calibrate and validate the numerical model. The aim of the laboratory experiments was to explore the optimal layout of pile groins, mainly under a combined wave-current flow condition.

In the present work, we set up a phase resolving wave-flow model SWASH (an acronym for Simulating WAves till SHore), which includes pile groin effects on the flow. The governing equations of this model are listed in Section 2 and the experimental data set is described in the same section. The initial calibration of the model is presented in Section 3. Then the model is applied to evaluate pile groin impacts on nearshore currents, which are demonstrated in the same section. Results are discussed in Section 4, and conclusions are given in Section 5.

2. Methods

2.1. Governing equations of SWASH

SWASH (Zijlema et al., 2011) is an open source flow-wave model which could simulate unsteady, non-hydrostatic free-surface flow and which has been successfully applied to study various wave dynamics nearshore on a laboratory scale (Zijlema et al., 2011; Smit et al., 2013; Rijnsdorp et al., 2017). Hereinafter brief introduction of the SWASH model is given. For details of the model, references are made to Zijlema and Stelling (2005, 2008), Zijlema et al. (2011) and Smit et al. (2013).

The governing equations are the RANS equations for an incompressible fluid including non-hydrostatic effects. In vertical direction, the water volume is bounded by the bottom $z = -d(x,y)$ and the free water surface $z = \zeta(x,y,t)$,where t is the time, and x, y and z are the Cartesian coordinates. The local continuity equation and momentum equations in a three-dimensional (3D) configuration are given as

$$\frac{\partial u_i}{\partial x_i} + \frac{\partial w}{\partial z} = 0 \tag{1}$$

$$\frac{\partial u_i}{\partial t} + \frac{\partial u_i u_j}{\partial x_j} + \frac{\partial u_i w}{\partial z} = -\frac{1}{\rho}\frac{\partial (p_h + p_{nh})}{\partial x_i} + \frac{\partial \tau_{ij}}{\partial x_j} + \frac{\partial \tau_{iz}}{\partial z} - f_i \tag{2}$$

$$\frac{\partial w}{\partial t} + \frac{\partial u_j w}{\partial x_j} + \frac{\partial w^2}{\partial z} = -\frac{1}{\rho}\frac{\partial (p_h + p_{nh})}{\partial z} + \frac{\partial \tau_{zj}}{\partial x_j} + \frac{\partial \tau_{zz}}{\partial z} - g \tag{3}$$

where i and j indicate two horizontal coordinates x/cross-shore and y/alongshore respectively, z is the vertical coordinate, u_i is the horizontal component of $\vec{u}$ in each direction, w is the vertical velocity, p_h and p_{nh} are hydrostatic and non-hydrostatic pressure components, respectively. The hydrostatic pressure p_h is explicitly expressed as $p_h = \rho g(\zeta - z)$, so $\partial_{x_i} p_h = \rho g \partial_{x_i} \zeta$ (where ∂_{x_i} stands for $\partial / \partial_{x_i}$), and $\partial_z p_h = -\rho g$ (where g is the gravitational acceleration). τ_{ij} are turbulent stresses. Equation (1) is the local continuity equation, and Equations (2) and (3) are momentum equations including the effects of mixing, bottom friction and resistance of cylinders. The last sink term of Equation (2) is the momentum loss due to the presence of PPG cylinders.

Integrating the local continuity equation in vertical direction, by substituting kinematic boundary conditions at free surface and impenetrable bottom, a global continuity equation is induced

$$\frac{\partial \zeta}{\partial t}+\frac{\partial}{\partial x_i}\int_{-d}^{\zeta} u_i dz=\frac{\partial \zeta}{\partial t}+\frac{\partial hU_i}{\partial x_i}=0 \tag{4}$$

where h (= $\zeta + d$) is the total water depth.

The bottom friction at the bottom boundary is computed according to the logarithmic law of the wall with a roughness height k_s (Launder and Spalding, 1974).The roughness height for a smooth concrete bottom used in laboratory experiment was chosen by calibration. The turbulence stresses are given based on eddy viscosity closure equations. The horizontal viscosity and vertical viscosity are estimated by the Smagorinsky type model (Smagorinsky, 1963) and the k- ε model (Launder and Spalding, 1974), respectively. The inclusion of vertical mixing spreads the effect of the bottom stress over the water column in vertical direction.

To account for the momentum lost due to the resistance of pile cylinders, a sink term is added to the right-hand side of equation (2), which consists of a nonlinear quadratic drag loss term

$$f_i=\frac{1}{2}NDC_D u_i|\vec{u}| \tag{5}$$

where C_D is the drag coefficient, N is the number of cylinder per unit bed area ($/\ m^2$) , D is the cylinder diameter (m), f_i is the density-normalized drag force per cylinder height in x/cross-shore or y/alongshore direction.

2.2. Performance metrics

Three objective functions, Root Mean Square Error (RMSE), Scatter Index (SI) and correlation coefficient R^2, were applied to evaluate the performance of the model, compared to the measurement data. The interested wave height H, mean water level $\overline{\eta}$ and mean longshore current velocity $\overline{V}$ are substituted by a variable f in the flowing equations, where 'o' is short for observation and 'c' is short for calculation.

$$\mathrm{RMSE}=\sqrt{\frac{1}{N}\sum_{i=1}^{N}\left(f_c^i-f_o^i\right)^2} \tag{6}$$

$$\mathrm{SI}=\frac{\sqrt{\frac{1}{N}\sum_{i=1}^{N}\left(f_c^i-f_o^i\right)^2}}{\overline{f_o}} \tag{7}$$

$$R^2=\frac{\sum_{i=1}^{N}\left(f_c^i-\overline{f_c}\right)\left(f_o^i-\overline{f_o}\right)}{\sqrt{\sum_{i=1}^{N}\left(f_c^i-\overline{f_c}\right)^2}\sqrt{\sum_{i=1}^{N}\left(f_o^i-\overline{f_o}\right)^2}} \tag{8}$$

2.3. Experimental arrangement

The data set, which was obtained by Hulsbergen and ter Horst, 1973 experiments (hereafter H73 in short), is utilised to compare with the simulation results. The aim of the scaled experiment was to examine the reduction extent of longshore currents due to the presence of PPGs with various layouts. The available experimental data are important to validate the implementation of pile groins in the numerical model and further test the interactions between pile groins and longshore currents.

A series of physical experiments were conducted in the 31.25 m long and 12.1 m wide wave basin of Delft Hydraulics in 1973, with the aim to investigate the optimal layout of a pile groin system. The bottom was made of smooth concrete and its contour is straight and parallel to the shoreline. The beach slope is 1/35 nearshore and 1:20 offshore (Fig. 4, c). For the simulations by the SWASH model, two representative layouts are chosen to be simulated: three 5 m long PPGs at a 10 m spacing alongshore and five 3.5 m long PPGs at a 5 m spacing alongshore, respectively, both consist of two rows of wooden cylinders. The two pile rows of a PPG are at a 0.0875 m alongshore interval. All the PPGs are perpendicular to the coastline. Given the geometric scaling of 1:40, the

Table 1
The parameters of the experiments.

Environmental parameters					
H_1 (m)	T_1 (s)	Θ_1 (°)	d_1 (m)	L_1 (m)	H/L_1
0.03	1.04	15	0.3	1.45	0.021
Pile groin configurations					
D (m)	P (%)	L_g (m)	X_g (m)	Num.	Groin type
0.006	50%	3.5	5	5	Double-row
0.006	55%	5	10	3	Double-row

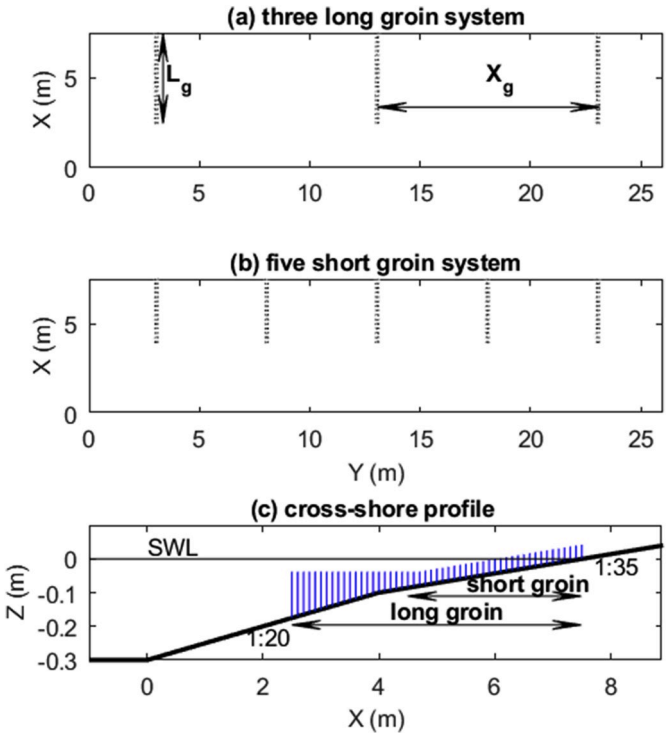

Fig. 2. The layouts of groin systems (a: three long groin system; b: five short groin system) and the cross-shore profile of groins.

pile rows are 200 m and 140 m long respectively on a prototype scale. Each pile row of the long groin consists 373 wooden dowels, while the short row consists of 292 dowels. The permeability values are varying across shore from a low permeability at the landward end to a high permeability at the seaward head of groins. Here permeability is defined as the ratio of cross-sectional void area to the total lateral profile area of a PPG, when viewed from the side. When the pile cylinders are spaced cross-shore equidistantly, the permeability could calculated by the ratio of the cross-shore interval between each pile cylinder over the summation of the interval and the pile cylinder diameter. In this study, the average permeability is 55% of long groins and 50% of short groins.

The hydraulic condition selected to be investigated in this paper is a combined wave-current condition, consisting of obliquely incident waves and alongshore steady currents. The pure current condition and pure wave condition are shown in Fig. 3 to demonstrate their characteristics separately. For the pure current condition, a constant discharge of 450 L/s imposed at the lateral boundary driving a steady current to flow alongshore (from the left to the right in Fig. 3 (a1),). The magnitude of the steady current is proportional to the square root of water depth $\sqrt{h}$, decreasing gradually from deep water to shallow water on the beach slope (Fig. 3 (a2),). When the water depth h is larger than 0.05 m, the Reynolds number ($Re_c = V_c h/\nu$) is beyond the threshold of 2 100 and the current is turbulent. The monochromatic unidirectional incident wave with H = 0.03 m and T = 1.04 s was generated approaching the shore at

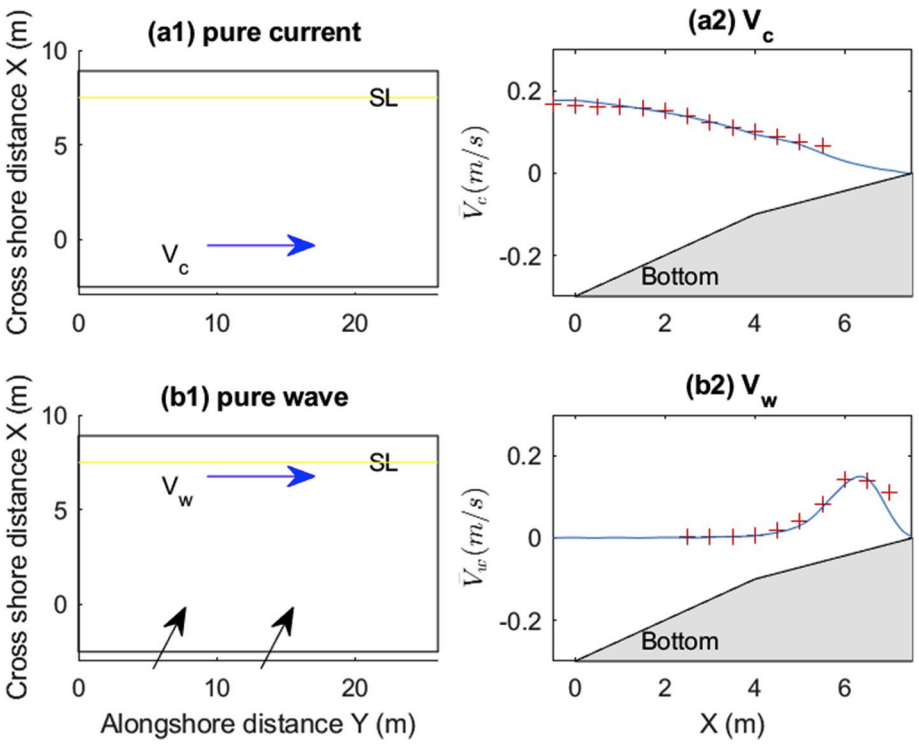

Fig. 3. The pure current condition: (a1) steady current direction (blue arrow), (a2) steady current velocity V_c; the pure wave condition: (b1) wave direction (black arrow), and wave induced alongshore current direction (blue arrow), (b2) wave induced current velocity V_w.. The red pluses denote the measured current velocity in the experiment, and the blue lines show the calculated current velocity, SL is short for shoreline. (For interpretation of the references to colour in this figure legend, the reader is referred to the Web version of this article.)

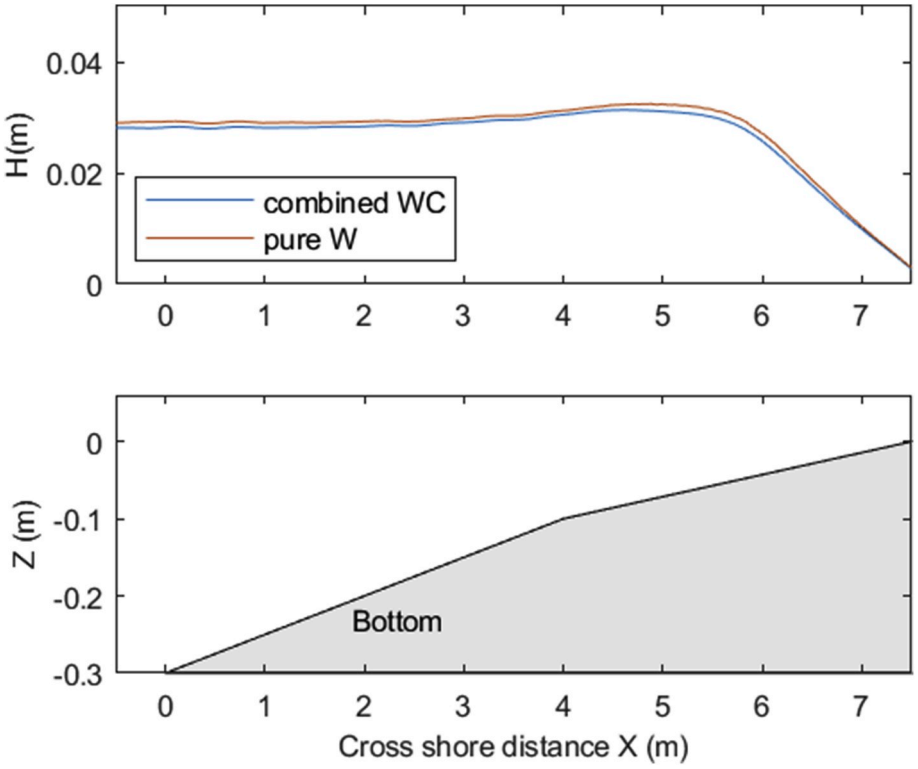

Fig. 4. The calculated wave height evolution in cross-shore direction, (a): wave heights, blue line shows the combined wave current condition, red line shows the pure wave condition; (b): bottom slope. (For interpretation of the references to colour in this figure legend, the reader is referred to the Web version of this article.)

an incidence angle of 15° to the shore normal direction (Fig. 3, b(1)). Given the combined wave current condition, wave-generated longshore currents are dominant within the breaker zone and flow in the same direction as the steady currents. Therefore, the superimposed longshore current near shore is enhanced and stronger than that under a pure wave or a pure current condition. When waves approach the shore, waves refract to shore normal direction, changing from a 75° intersection angle to alongshore steady current direction at offshore boundary, to a near-orthogonal angle (81.5°) when waves are breaking. The steady current induced wave refraction was found insignificant in this case, less than

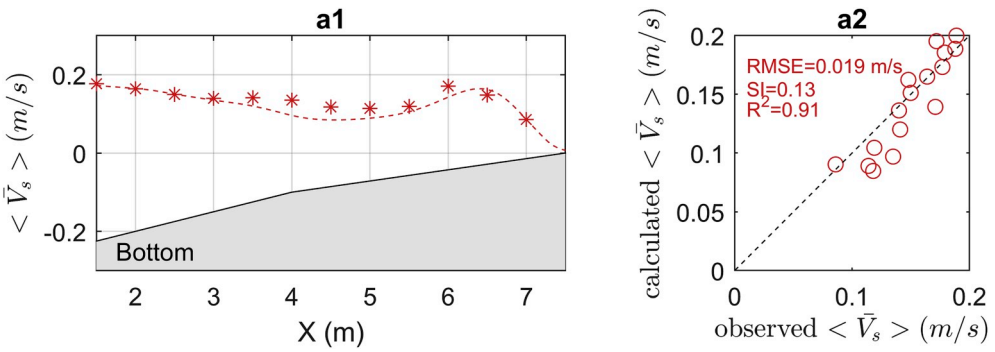

Fig. 5. The cross-shore distribution of longshore-averaged mean longshore currents $< \overline{V_s} >$ under combined wave current condition without groin existence, (a1: longshore current velocity magnitudes, the subscript 's' represents the velocities at the superficial layer and the triangular braces '< >' denotes for longshore averaging, red line: calculations, red starts: measurements; a2: model performance statistics, the black dashed line denotes a perfect agreement). (For interpretation of the references to colour in this figure legend, the reader is referred to the Web version of this article.)

3%. A summary of the test parameters is given in Table 1. The layouts of the two groin system and the cross-shore profile are denoted in Fig. 2.

2.4. Numerical implementation

To set up the model for H73 experiments, the physical domain was discretised by a structured grid. The grid resolution was constant, which was $\Delta x = 0.03\ m$ in cross-shore direction and $\Delta y = 0.1$ m in alongshore direction (resulting in 380 × 260 grid cells). Although a coarse vertical resolution (e.g. 2 layers) is sufficient to resolve wave physics (for instance wave propagation, shoaling, wave breaking and wave run-up), a very fine vertical resolution (~10–20 layers) is required to well represent wave breaking dissipation in the surf zone (Smit et al., 2013). In this study, the vertical layers were chosen to be 15 equidistant layers, which was proved to be fine enough (see the following section) to capture the proper magnitudes of longshore currents. The time step was set at $\Delta t = 0.005$ s. Cyclic boundaries were used at lateral boundaries to limit the length of an unbounded coast. The obliquely incident regular waves were generated at the offshore open boundary. In addition to the waves; a constant water level gradient 3.1×10^{-5} at the lateral flow boundaries was exerted to mimic the steady longshore currents in the laboratory. The implementation of the longshore water level gradient is included in a modified version of SWASH (De Wit et al., 2017).

To represent the PPG, we do not resolve the pile cylinders in the SWASH model. It is assumed that the cylinders are uniformly distributed within the volume between the two parallel pile rows of each PPG. We set the alongshore grid resolution approximately equal to the width of a PPG, thus pile cylinders spread uniformly within one grid cell alongshore. Given the cylinder diameter D = 0.006 m and the wave length λ = 1.45 m, resulting in a ratio of D/λ much smaller than the order of O (0.1), the pile cylinders could be seen as slender cylinders. Therefore the spatial variation of the undisturbed flow near cylinders within computational grid cells is assumed to be neglected. The projected area of the uniformly distributed PPG (udPPG) should be equal to that value of the real PPG, to guarantee the total drag forces are same. Thus, the frontal area $A_f\ (= D\sum_{i=1}^{n} h_{g,i})$ of a PPG is equal to the value $A_{ud}(= N W_g L_g \overline{h_g} D)$ of

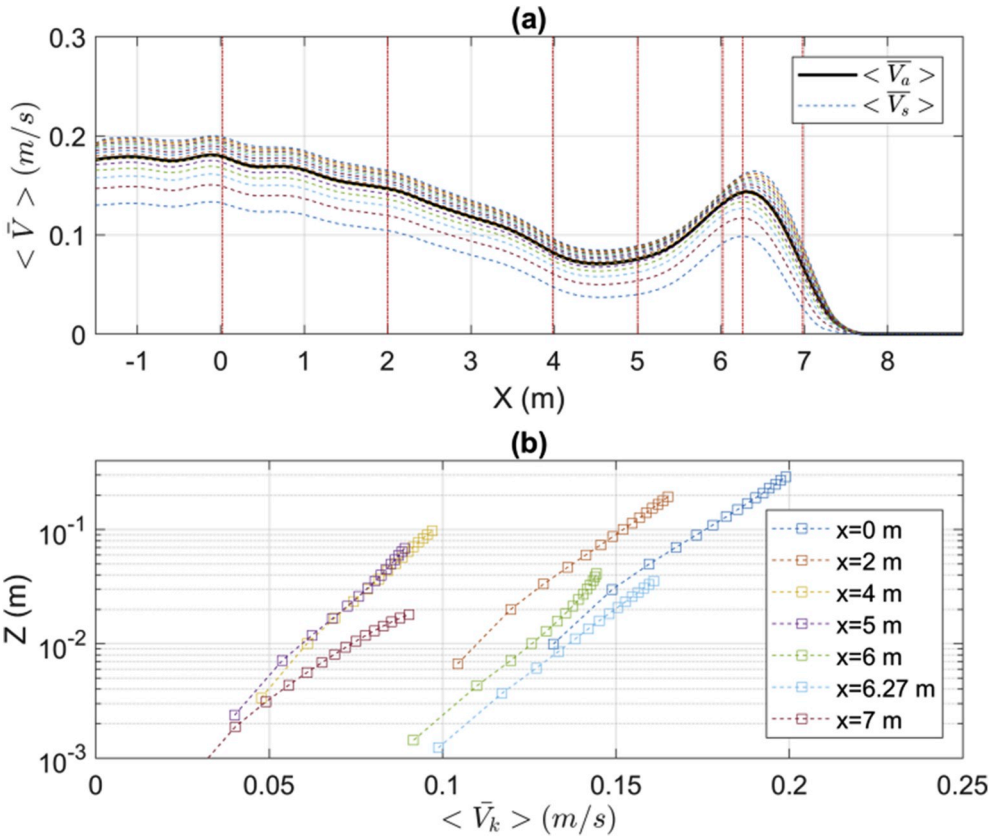

Fig. 6. The predicted vertical structure of mean longshore currents $< \overline{V} >$, ((a): cross-shore variations of longshore current velocity magnitudes, dot lines: longshore current velocities $< \overline{V_k} >$ at each layer centre; black solid line: depth averaged longshore current velocities $< \overline{V_a} >$; red vertical lines: selected positons where the vertical variations of longshore current are shown in the bottom figure (b). (b): the vertical variations of layered longshore current velocities $< \overline{V_k} >$ at 7 selected cross-shore locations.). (For interpretation of the references to colour in this figure legend, the reader is referred to the Web version of this article.)

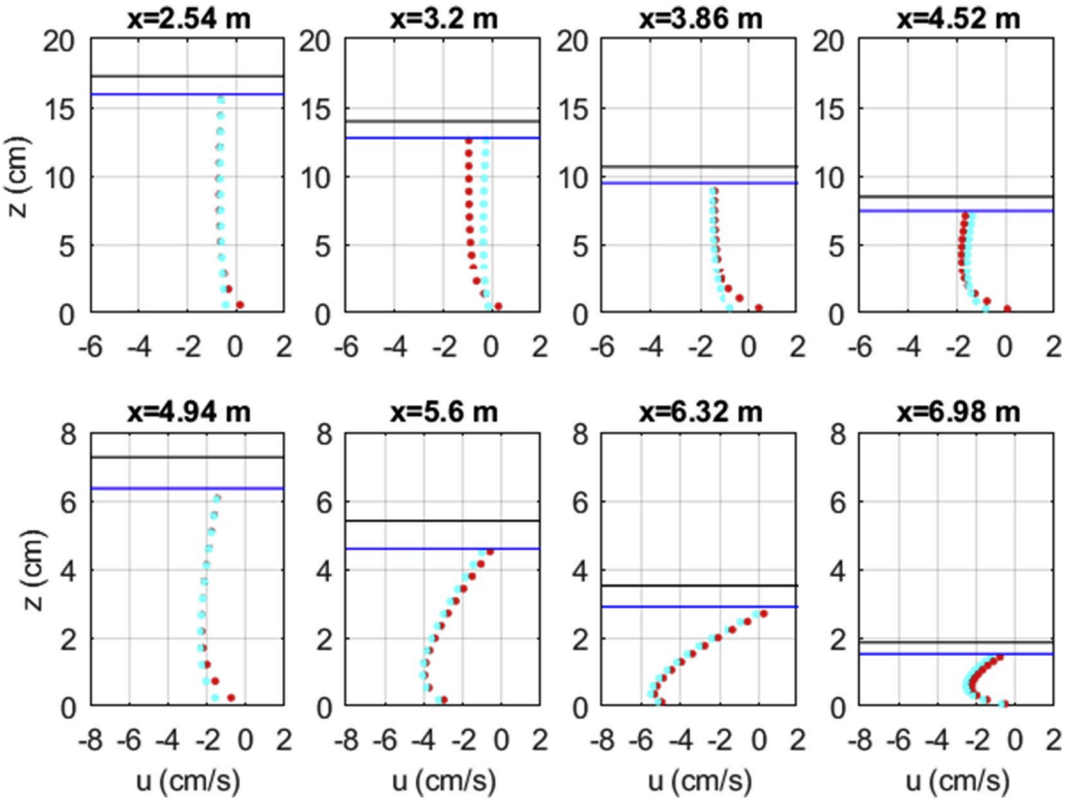

Fig. 7. The predicted vertical structure of mean cross-shore shore return currents $< \overline{u} >$ under wave trough at 8 selected cross-shore locations, red dots display the pure wave condition and the cyan dots the combined wave current condition, the four subplots on the upper panel are locations outside the breaker zone, while the four subplots on the lower panel are inside the breaker zone, the blue lines represent the wave trough, and the black lines indicate still mean water level. (For interpretation of the references to colour in this figure legend, the reader is referred to the Web version of this article.)

a udPPG, where D is the diameter of a pile cylinder, n is the total number of pile cylinders of each PPG, L_g is the groin length, W_g is the groin width, and N is the number of cylinders per unit area, $\overline{h_g}$ is the averaged groin height. The computed $\overline{h_g}$ is 0.0525 m of short groins and 0.06 m of long groins. The drag forces by the udPPG are computed from equation (5). The unknown drag coefficient C_D was derived through calibration, with the aim to obtain computed longshore current velocities comparative with measured results, and having minimal root mean square errors against measurement data.

3. Results

In this section, the simulation results of H73 experiments are presented. The groinless base experiment is used to test the ability of predicting accurate longshore currents of SWASH model on a laboratory scale. The bottom friction coefficient was calibrated under combined wave-current flow. For the combined wave-current condition concerned in this study, the bottom roughness height was calibrated in the range of 0.0004 m–0.001 m, and chosen to be 0.0008 m for which the minimal root mean square error was obtained. Then to calibrate the drag coefficient of udPPG, three 5 m long groins are introduced in the bottom roughness calibrated flow model. The drag coefficient is set as 1.1 calibrated in the range of 0.8–1.4. The calibration results of bottom roughness and drag coefficient are described in appendix A. Finally, the calibrated udPPG model was used to validate the hydrodynamics of another groin system consisting of five 3.5 m short groins.

3.1. *Hulsbergen et al. (1973) Experiments*

3.1.1. *Groinless bare bottom*

When the groins are not involved in the numerical model, the model was calibrated to reproduce the observed wave height and longshore current variations in the experiments. Compared to measured longshore current velocities, the simulations produced good results under the pure wave condition (Fig. 3 (a2),) and the pure current condition (Fig. 3 (b2),). Then, the SWASH model succeeded in simulating the complex combined wave current condition (Figs. 5–6). The calculated maximal wave height is 0.033 m (Fig. 4), which is consistent with the measured breaking wave heights ranging from 0.025 to 0.035 m.

The calculated mean longshore current velocities at the first superficial layer of the water volume are shown in Fig. 5, where the subscript 's' represents the superficial and the triangular braces '< >' denotes for longshore averaging. The thickness of each equidistant layer equals to 1/15 of the total water depth. The aim of the choice of superficial $\overline{V_s}$ is to be consistent with the observed mean longshore current velocities measured by surface floaters in the experiment. The simulation results agree well with the measurements (Fig. 5, a1). For instance, good agreements are observed within the inner breaker zone where the wave-induced longshore currents are dominant (X = 5.5 m to X = 7.5 m, in Fig. 5 a1) and in the seaward zone where steady currents are dominant (X = 1.5 m to X = 3 m, in Fig. 5, a1). In the transition zone, the model underestimates the currents somewhat. The statistic indexes for the calculations, for instance, the scatter index is 0.13 and the correlation coefficient is 0.91 (Fig. 5, a2), show a reliable reproduction of the measured longshore current velocities. The root mean square error (RMSE) of the calculated longshore currents $\overline{V_s}$ is 0.019 m/s.

Within the breaker zone, the maximal combined longshore current velocity increases by 14% compared to that under the pure wave condition, but its location doesn't change, both are at 1.18 m seaward shoreline (X = 6.32 m, in Fig. 3, b(2), and Fig. 5, a1). Unfortunately, there is no available information about vertical variations of longshore currents from the experiment. We present the predicted vertical

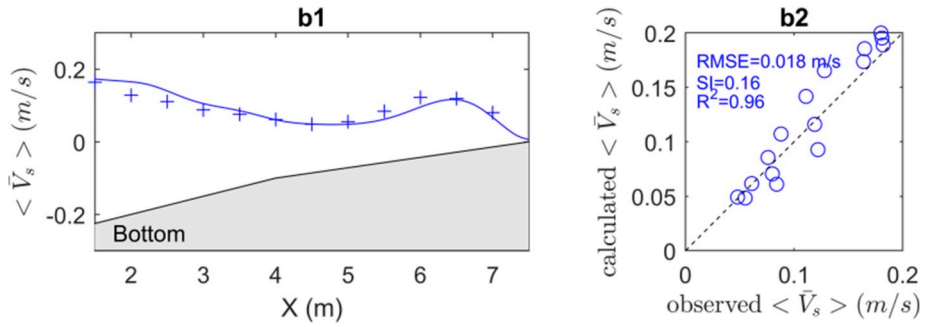

Fig. 8. The cross-shore distribution of $< \overline{V_s} >$ (longshore averaged in three-groin fields), (b1: longshore current magnitudes, the subscript s denotes the velocities are at the superficial layer; blue line: calculations, blue pluses: measurements; b2: model performance statistics, the black dashed line denotes a perfect agreement). (For interpretation of the references to colour in this figure legend, the reader is referred to the Web version of this article.)

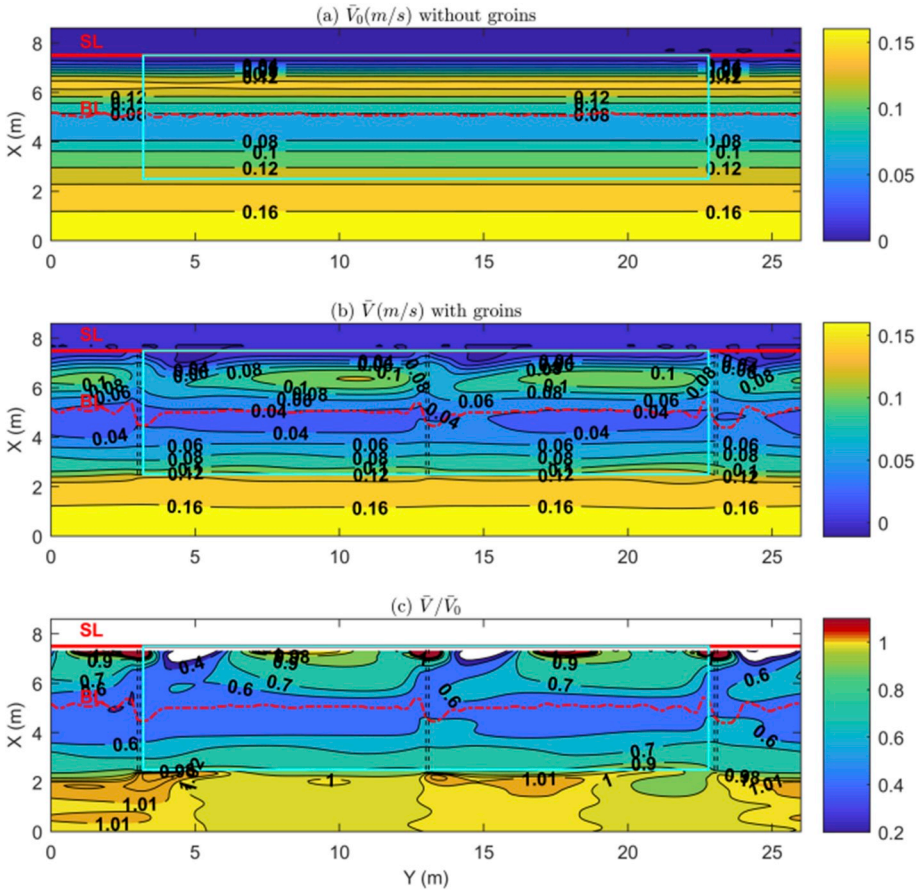

Fig. 9. The mean depth-averaged longshore current flow fields affected by three long groins, (a: $\overline{V}_0$ without groins; b: $\overline{V}$ with three long groins; c: only positive normalized longshore current velocity magnitudes $\overline{V}/\overline{V_0}$ are shown, the ratio values were excluded if V_0 is less than 1 cm/s near shoreline; black dash lines denote the locations of three long groins, cyan solid rectangles show the groin fields, red solid lines denote the shoreline (SL), and red dot lines denote the wave breaker lines (BL)). (For interpretation of the references to colour in this figure legend, the reader is referred to the Web version of this article.)

structures of longshore currents at 7 selected positions cross-shore in Fig. 6. It could be seen that the vertical longshore current profiles are nearly linear in the semi-log plot, which means they could be well described by a logarithmic profile. Considering the return current under the wave trough in cross-shore direction (Fig. 7), its vertical structure shows two distinct kinds of profiles. Outside the breaker zone, the vertical profile of the return current has less curvature. While inside, the vertical profile turns to be very curved with a dominant seaward velocity near bed and a weak seaward flow or shoreward flow at the wave trough level. Such remarkably different features are consistent with observations in laboratory (e.g. Nadaoka and Kondoh, 1982), and could be well predicted by mathematical models (e.g. Putrevu and Svendsen, 1993). Compared with the pure wave condition outside the breaker zone, the return current profile become less curved when superimposed by nearly orthogonal currents (the up panel in Fig. 7). Inside the breaker zone, the presence of currents does not alter the vertical profile, only the magnitudes slightly increase but could be ignored (the lower panel in Fig. 7).

3.1.2. *Three long groin system*

The calculated longshore currents (averaged in longshore direction within the three-groin field from Y = 3 m to Y = 23 m) match well with experiment data measured by surface floaters flowing through three-groin field (Fig. 8). The existence of groins retarded longshore currents within the three groin fields (Fig. 9). Compared with the non-groin longshore current field (Fig. 9, a), the groin-interfered longshore currents are less uniform within the breaker zone (Fig. 9, b). The reason for this is that when longshore currents flow down drift the leeside of PPGs, they immediately gain energy from the breaking waves intruding into

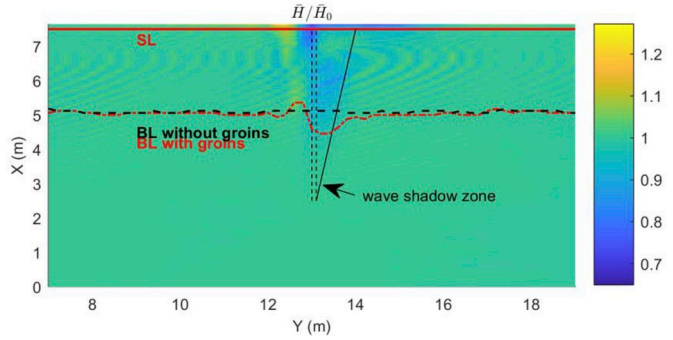

Fig. 10. The normalized wave height $\overline{H}/\overline{H_0}$ near the middle groin of a three-groin system (black line: breaker line without groins, red line: breaker line with groins). (For interpretation of the references to colour in this figure legend, the reader is referred to the Web version of this article.)

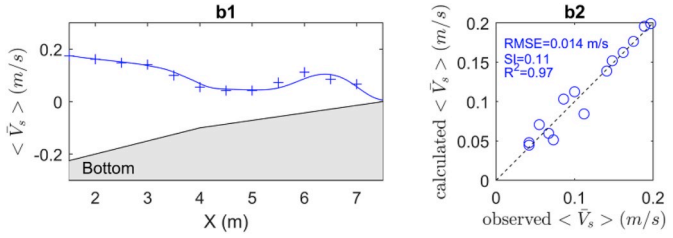

Fig. 11. The cross-shore distribution of $< \overline{V_s} >$ (longshore averaged in five-groin fields), (c1: longshore current magnitudes, the subscript s denotes the velocities are at the superficial layer; blue line: calculations, blue pluses: measurements; c2: model performance statistics, the black dashed line denotes a perfect agreement). (For interpretation of the references to colour in this figure legend, the reader is referred to the Web version of this article.)

the area. However, at the seaward breaker zone, where the steady currents (representing tidal currents but seen as steady currents in the laboratory) are dominant and intercepted by PPGs, the currents recover gradually from the diffusion of mass and momentum from the main stream (Bakker et al., 1984). The difference between the generation mechanism of steady currents and wave-induced currents explains the uniformity outside the break zone and the non-uniformity within the breaker zone respectively (Fig. 9, c). It is clearly shown in Fig. 9 (b) that the magnitudes of longshore currents quickly reduce when passing through a groin and only recover flowing further down drift the groin.

Although pile groins could efficiently retard wave-induced longshore currents, they appeared to hardly attenuate wave energy. This is because groin width is much smaller compared to incident wave length, for the considered case, the ratio is little more than 0.06. Fig. 10 shows the wave height distribution near the middle groin of the three-groin system. When waves approach the groin, the wave heights increase slightly, then reduce to minimal values at the groin locations. The increase of wave height updrift the groin and the decrease of wave height downdrift at the obliquely incident wave shadow zone could be ignored given their limited affected area just around the groin location.

3.1.3. Five short groin system

The longshore current velocities are more efficiently reduced within five short groin fields compared with the three-groin system, as the average resistance to the flow increased by two additional pile groins. Within the breaker zone, the maximal magnitude of longshore current velocities is 0.098 m/s (Fig. 11), while is 0.11 m/s when the flow is hindered by three long groins (Fig. 8), compared with 0.17 m/s without interceptions of groins (Fig. 5). Similar to the three-groin system, the five-groin system produced a comparable pattern of longshore current fields as shown in Fig. 12. The normalized velocities are reduced to 0.4

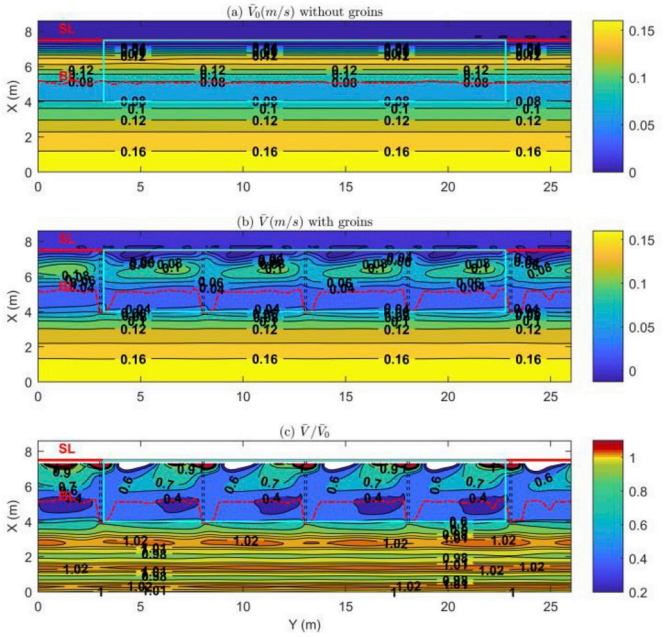

Fig. 12. The mean depth-averaged longshore current flow fields affected by five short groins, (a: $\overline{V}_0$ without groins; b: $\overline{V}$ with three long groins; c: only positive normalized longshore current velocity magnitudes $\overline{V}/\overline{V_0}$ are shown, the ratio values were excluded if V_0 is less than 1 cm/s near shoreline; black dash lines denote the locations of three long groins, cyan solid rectangles show the groin fields, red solid lines denote the shoreline (SL), and red dot lines denote the wave breaker lines (BL)). (For interpretation of the references to colour in this figure legend, the reader is referred to the Web version of this article.)

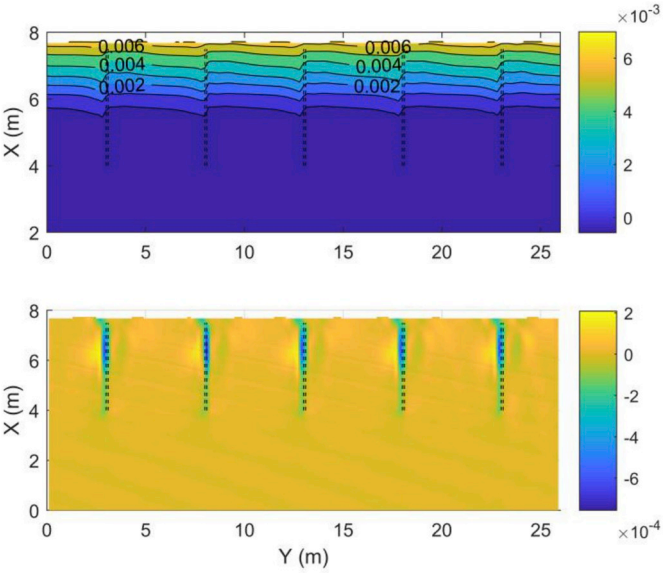

Fig. 13. The water level filed affected by five short groins. up: time averaged water level $\overline{\eta}$ (m); bottom: alongshore gradient of water level $\partial\overline{\eta}/\partial y$ (black dash lines denote the locations of groins).

to 0.7 within five short groin fields (Fig. 12, c) while such velocities are 0.6–0.9 within three long groin fields (Fig. 9,c).

When groins are dense along a uniform coast, the groin interference induced the non-uniformity of the water level. For the five groin system, the water level variations are illustrated in Fig. 13. The mean water level field is generally uniform. The contour lines are unparalleled to the

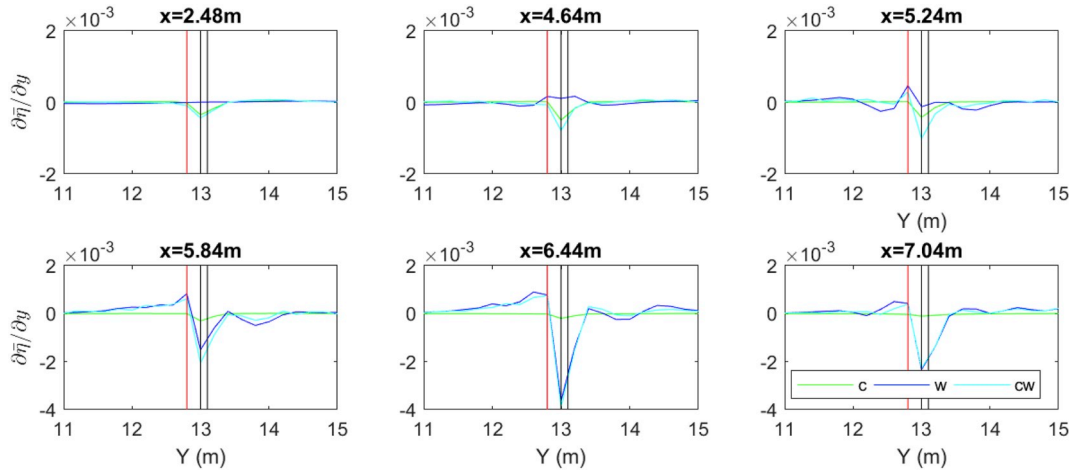

Fig. 14. The alongshore water level gradient $\partial\overline{\eta}/\partial y$ under three conditions, at 0.2 m updrift the middle groin of the three long groin system (denoted by the red lines).The black lines represent the middle pile groin location. c is short for the pure current condition, w for pure wave condition, and cw is for combined current wave condition. (For interpretation of the references to colour in this figure legend, the reader is referred to the Web version of this article.)

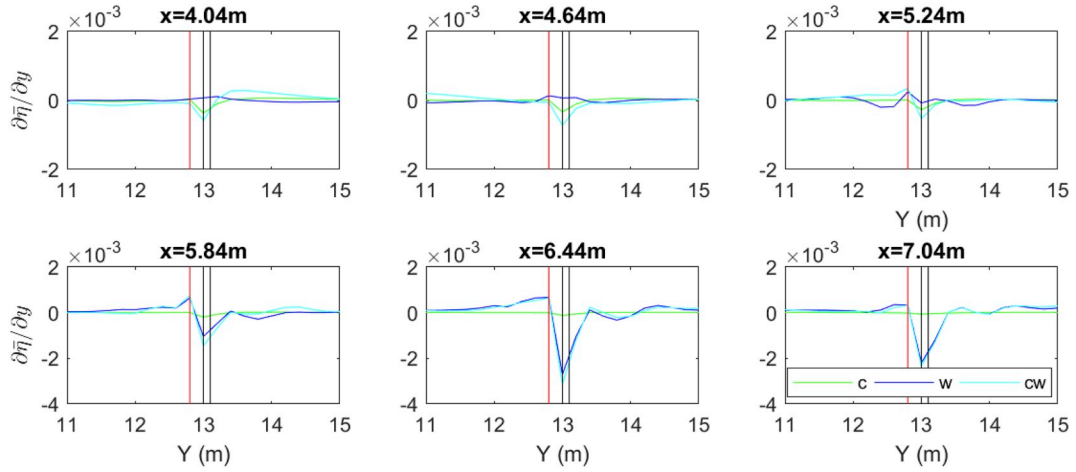

Fig. 15. The alongshore water level gradient $\partial\overline{\eta}/\partial y$ under three conditions, at 0.2 m updrift the middle groin of the five short groin system (denoted by the red lines). T he black lines represent the middle pile groin location. (For interpretation of the references to colour in this figure legend, the reader is referred to the Web version of this article.)

shoreline, due to the increase of the water level updrift a groin and the decrease of water level downdrift a groin. The bottom plot of Fig. 13 demonstrates that the local alongshore water level gradients nearby groins are at the order of O(10^{-4}). The local water level gradient is larger than the global water level gradient, which is at the order of O(10^{-5}).

4. Discussion

4.1. Wave height $\overline{H}$

Theoretically, there are four kinds of wave components within groin fields: incident, diffracted, reflected and transmitted waves. Considering the small incident angle of waves, the waves could propagate into nearly the total groin fields. The diffraction of waves around groins is not obvious, because the limited interference by a very narrow width of groin piles and the littoral currents flowing through groin openings eliminate the diffraction effects. Slightly enhanced wave height is observed updrift groins (Fig. 10), due to the water level is piled up updrift the groins and consequently wave breaking is delayed. In addition to the slightly enhanced wave height updrift the groins, the wave height reduction (20% at maximal under 15° incident regular waves) of transmitted waves occurs within the obliquely incident wave shadow zone. The moderate wave dissipation confined to the very limited area reveal that the effects of such pile groins on waves are of no consequence and negligible. The negligible effects of pile groins on waves are consistent with the views of Raudkivi (1996) and other researchers. Therefore, the wave height variation in pile groin fields is needless to be further discussed.

4.2. Water level $\overline{\eta}$

The water level field is generally uniform alongshore except in the narrow areas near both flanks of a groin. The resistance exerted to longshore flow by groins piled up the water level updrift the groins and produced a water level differential within groin fields. The water level variation $\Delta\overline{\eta}$ in alongshore direction near the groins is at the order of O(10^{-4}) m. Given the narrow width of pile groin O(10^{-1}) m, the water level gradient near groins is up to O(10^{-3}). In the simulation, the local water level gradient induced by groins is larger than the global water level gradient O(10^{-5}). The water level gradients were shown in figures (Fig. 14 and Fig. 15). The piled up water updrift the groins induces an alongshore positive water level gradient. The positive water level gradient drives forces opposite to the currents which are flowing in the positive Y direction. It is shown that, within the breaker zone, the

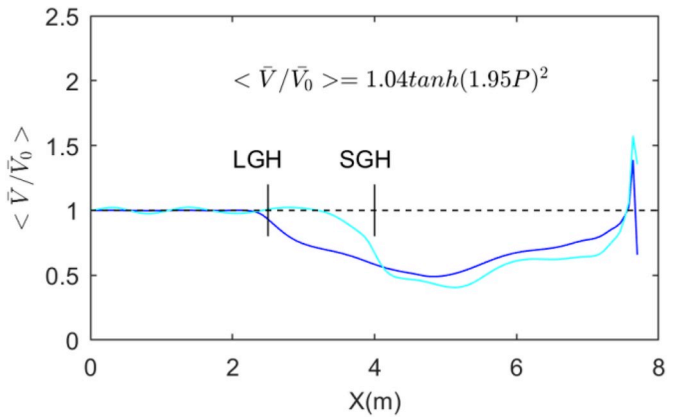

Fig. 16. Normalized longshore current $< \overline{V}/\overline{V_0} >$ longshore averaged in groin fields under combined wave current condition. (blue line: five-groin field, cyan line: three-groin field, black line: short groin head (SGH) location and long groin head(LGH) location, P is short for groin permeability). (For interpretation of the references to colour in this figure legend, the reader is referred to the Web version of this article.)

magnitude of $\partial\overline{\eta}/\partial y$ near the middle groin (three long groins in Fig. 14 and five long groins in Fig. 15) are nearly the same under wave and combined current wave conditions. Its order is $O(10^{-3})$, much larger than that of $O(10^{-4})$ under pure current condition. Therefore, the reduction effect of longshore current within the breaker zone is dominated by wave induced forces. However, outside the breaker zone at the groin location, the pure waves induced $\partial\overline{\eta}/\partial y$ decrease rapidly and shift from negative to positive in a seaward direction. In contrast, the $\partial\overline{\eta}/\partial y$ under pure current condition increases and keeps negative, and its magnitudes become larger than that under pure wave condition. Therefore, outside the breaker zone, the effects of waves and currents on longshore current variations are opposite.

4.3. Longshore current $\overline{V}$

In this paper, numerical simulations showed that the presence of permeable groins effectively reduces longshore currents (Figs. 9 and 12, Fig. 14 and 15) under different hydraulic conditions, as demonstrated by measurements in laboratory experiments (Hulsbergen and ter Horst, 1973). The relative longshore current velocities ($\overline{V}/\overline{V_0}$) are less than one within groin fields (Figs. 9 and 12). The relative velocities ($\overline{V}/\overline{V_0}$) are slightly larger than one near the long groin seaward heads (Fig. 9), while its value is less than one around the short groin seaward head (Fig. 12). This is partly because the current (V= 0.13 m/s) at further 5 m offshore long groin head location is 1.6 times stronger than that at 3.5 m offshore short groin head location. The current streamlines deflect and contract nearby the long groin heads, which enhances the local current velocity and compensates the reduction induced by the pile groin resistance. Another reason could due to the difference of the water level gradient $\partial\overline{\eta}/\partial y$ around the groin heads. The $\partial\overline{\eta}/\partial y$ down drift the long groin heads are nearly zero (the first subplot in Fig. 14), while the gradients are positive downdrift the short groin heads (the first subplot in Fig. 15). The positive water level gradient induces pressure forces in opposite direction to longshore currents, therefore hinders longshore currents. On the other hand, the smaller groin gap of the short groin system limits the development of mixing layer and momentum exchange along the groin head contour.

An empirical formulation relating the groin permeability and the $< \overline{V}/\overline{V_0} >$ averaged over the groin field was given in Fig. 16, followed by the suggested form raised by Trampenau et al. (2004). The relative velocity $< \overline{V}/\overline{V_0} >$ reduced to 67% within the three long groin field of a 55% permeability and to 57% within the five short groin field of a 50% permeability. The empirical formulation shows the nonlinear relation between longshore current reduction and groin resistance (by groin permeability). However, it could be only used to give a quick prediction, since the whole groin filed averaged values disguises detailed local information.

Near the groin shoreward ends, the relative velocities $< \overline{V}/\overline{V_0} >$ increase more than 1.5 times. At the wave set up location, the relative longshore current even increases by an order of magnitude (the 0.02 m shoreward the still water line in Fig. 17). But such sharp change is only limited to 1 m updrift the groin, and the strength of longshore currents is quite weak due to very shallow water depth near the shoreline. Such weak currents do not harm the beach and do not need extra considerations under mild waves. However, when extreme water level surges occur, the large inundation water depth on the beach allows strong

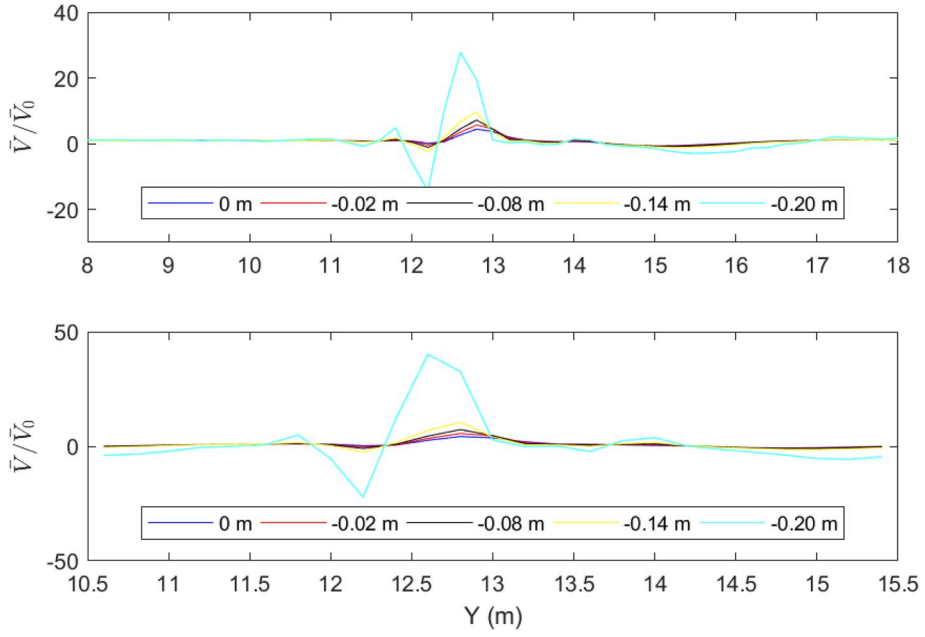

Fig. 17. The relative longshore current $\overline{V}/\overline{V_0}$ zoom in the middle groin shoreward end. (up panel: long groin system, bottom panel: short groin system.). The legend shows the shoreward distance from the still water line.

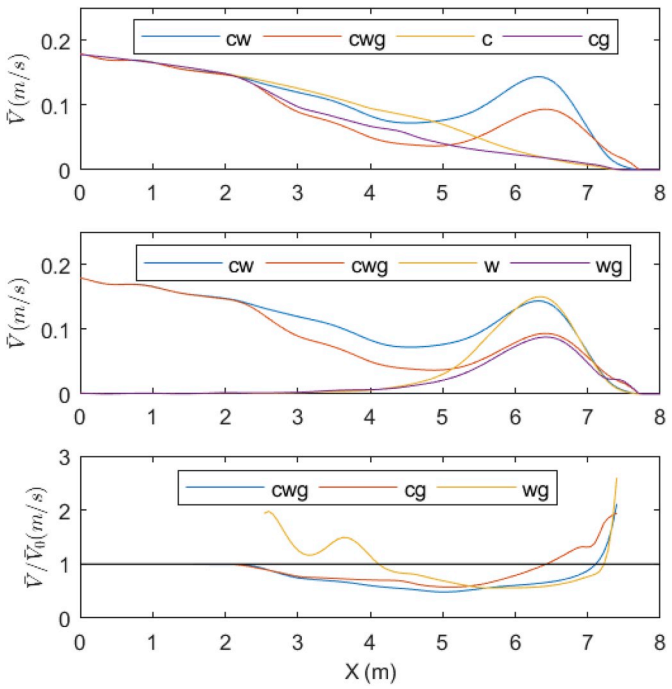

Fig. 18. The cross shore profiles of mean longshore current $\overline{V}$ under three conditions, at 0.2 m updrift the middle groin of the three long groin system. (cw is short for the combined current wave condition without groins, c for the pure current condition, w for the pure wave condition, wg and cg for pure wave condition with groins and pure current with groins separately.)

longshore currents to develop. The strong longshore current causing outflanking by groin ends to erode the beach or the shoreward dune foot if close enough could be affected. For instance, the beach slope has been eroded at shoreward ends of PPGs at Warnemünde, Germany, observed by Trampenau et al. (1996). The contracted strong longshore currents could even wash out the pile cylinders during storm surges, which is the main cause of failures of PPGs recorded in the Netherlands (Bakker et al., 1984). Therefore, the shoreward extension distance of PPGs from the shoreline deserves serious consideration, and the predictions by numerical simulations under extreme design scenarios maybe helpful to decide an appropriate shoreward length of a PPG. The extension distance should be at least shoreward beyond the wave set up line. If the dune foot erosion induced by outflanking flow should be avoided, the groin length has to extend to the dune foot location.

To isolate the waves and currents effects on longshore current reduction, we compare the cross distribution of longshore current under combined current wave condition, pure wave condition and pure current condition in Fig. 18. The chosen cross shore profile is at 0.2 m updrift the middle groin of the three long groin system. Under combined wave current condition, with the existence of currents, the reduction of longshore current is slightly smaller than that under pure wave condition, within the breaker zone; while the reduction is nearly same as that under pure current condition, outside the breaker zone. The reason of the difference in the reduction between X = 4 m and X = 5 m is hard to assess, for the simulation underestimates the longshore current velocities in this area suggesting some uncertainty exists. The upper panel in Fig. 18 shows that under pure current condition, $\overline{V}$ increases a little near shore (from X = 6.5 m to shoreline X = 7.5 m). The middle panel in Fig. 18 shows that under pure wave condition, $\overline{V}$ increases a bit near the shoreline (from X = 7.5 m to shoreline X = 7.7 m).

4.4. Cross-shore current $\overline{U}$

In addition to the distribution of longshore currents, the cross-shore return currents under wave trough within groin fields have been predicted and investigated. The existence of groins evokes rip currents near groin flanks. The intensity of rip currents updrift the groin is the strongest within surfzone. The values could maximally reach 0.06 m/s closely updrift the groins (Fig. 19) which is about 1.5 times the maximal return current 0.04 m/s without groin disturbance. Closely downdrift the groins, the maximal return current decreases a bit, and the locations

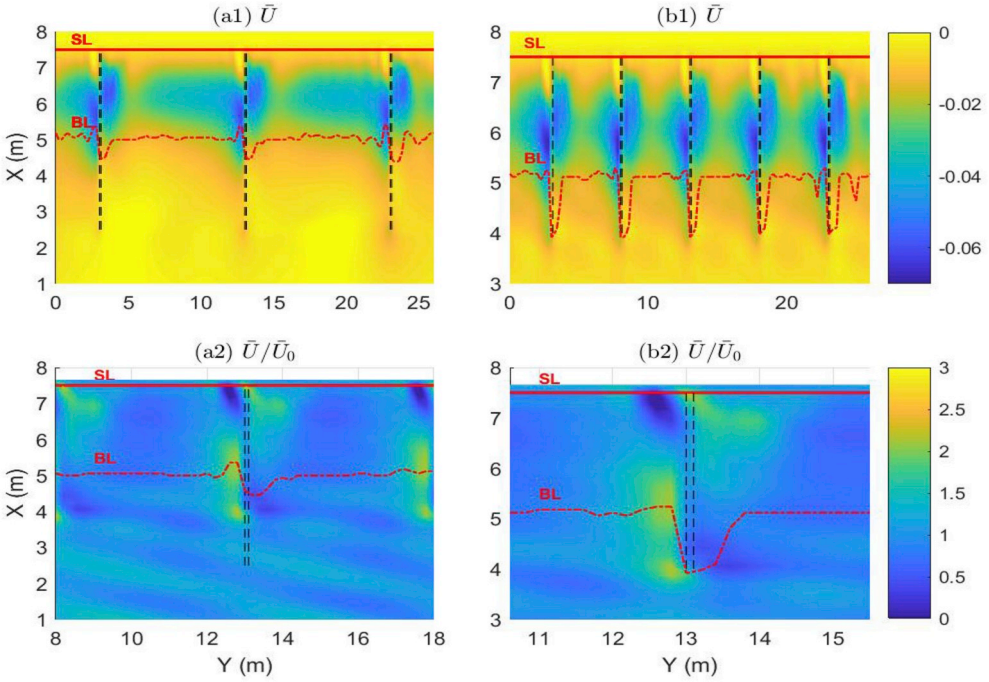

Fig. 19. The return current $\overline{U}$ (m/s) under wave trough in the presence of three 5 m long pile groins (a1), the relative return current $\overline{U}/\overline{U}_0$ (a2); the return current $\overline{U}$ in the presence of five 3.5 m short pile groins (b1), the $\overline{U}/\overline{U}_0$ (b2). Black dashed lines denote the pile groins, red solid lines denote the shoreline (SL). (For interpretation of the references to colour in this figure legend, the reader is referred to the Web version of this article.)

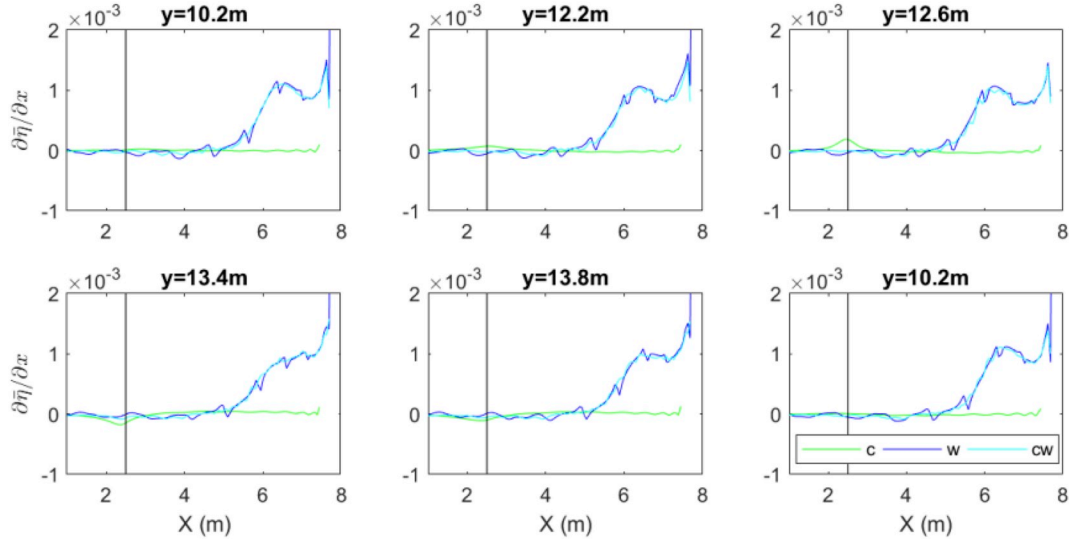

Fig. 20. The cross shore water level gradient ($\partial\,\overline{\eta}$)/∂x under three conditions, at three updrift (up panel) and three downdrift (bottom panel) the middle groin of the five short groin system. The black lines represent the pile groin head location. c is short for pure current condition, w for pure wave condition, and cw is for combined current wave condition, all the conditions are interfered by the groin system.

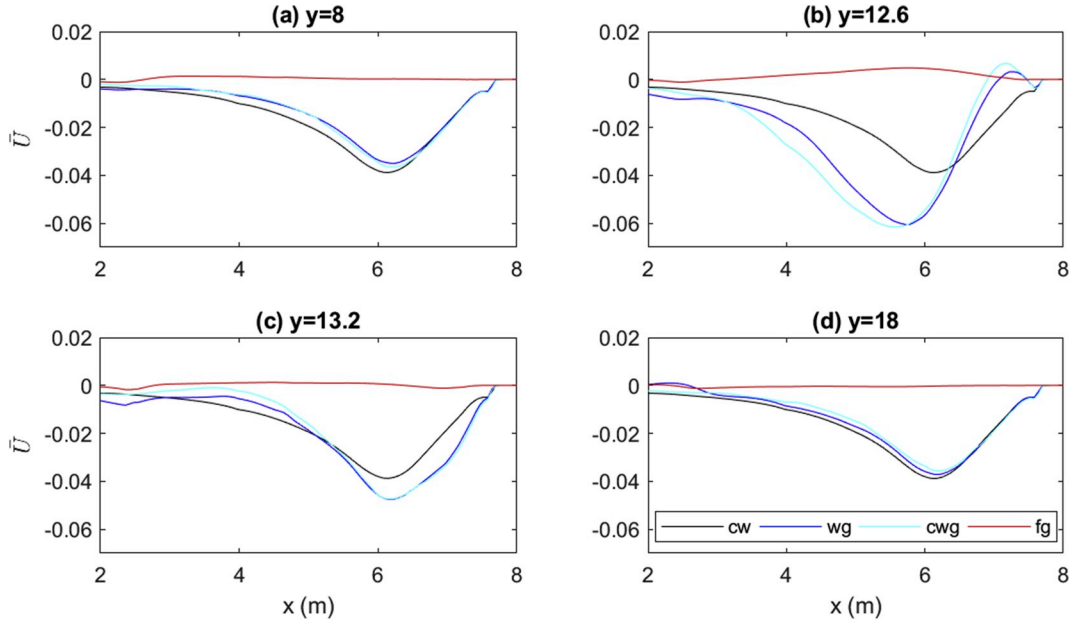

Fig. 21. The calculated return current $\overline{U}$ at four selected cross-shore locations near the middle groin of the three long groin system, ((a): half Xg updrift, (b):0.2 m updrift, (c): 0.3 m down drift, (d): half Xg downdrift). cg is short for pure current condition, wg for pure wave condition, cwg is for combined current wave condition, and cw is combined current wave condition without groin interference.

shift to shoreward (Fig. 21). The shoreward movement corresponds to the shoreward move of the peak of cross shore water level gradient (the subplot at y = 13.4 m Fig. 20). However, the maximal relative $\overline{U}/\overline{U_0}$ is at the wave breaker line position. The lowest mean water levels appear at the locations occupied by groins (e.g. Fig. 13). The greater water level gradients are consistent with the larger rip currents, updrift the groins and within the breaker zone (e.g. Fig. 19, a2, b2 and Fig. 20). Under the pure current condition, the rip current magnitude is much smaller than that under combined current wave condition (Fig. 21). Therefore the cross-shore current $\overline{U}$ is mainly dominated by the enhanced wave induced return current besides the groins.

Another characteristic of PPGs is the induced quite unidirectional flow field in permeable groin fields, compared to the nonuniform flow field in impermeable groin fields (Fig. 22). The high permeability of PPGs hinders the development of circulation and eddies in groin embayment and weakens the strength of rip currents updrift groins, compared to impermeable groins with the same configurations of a three long groin system.

4.5. Longshore volume discharge

The calculated alongshore discharge, the product of longshore current velocity and water depth, was denoted in Fig. 23. The maximal decrease of longshore volume discharge could reach 50% by three-groin and 40% by five-groin systems, compared with a shore without groins. It has been shown that the five-groin system reduced longshore volume discharge <q> is slightly higher than that by the three-groin system (Fig. 23) within the breaker zone, while the longer groins diminish <q>

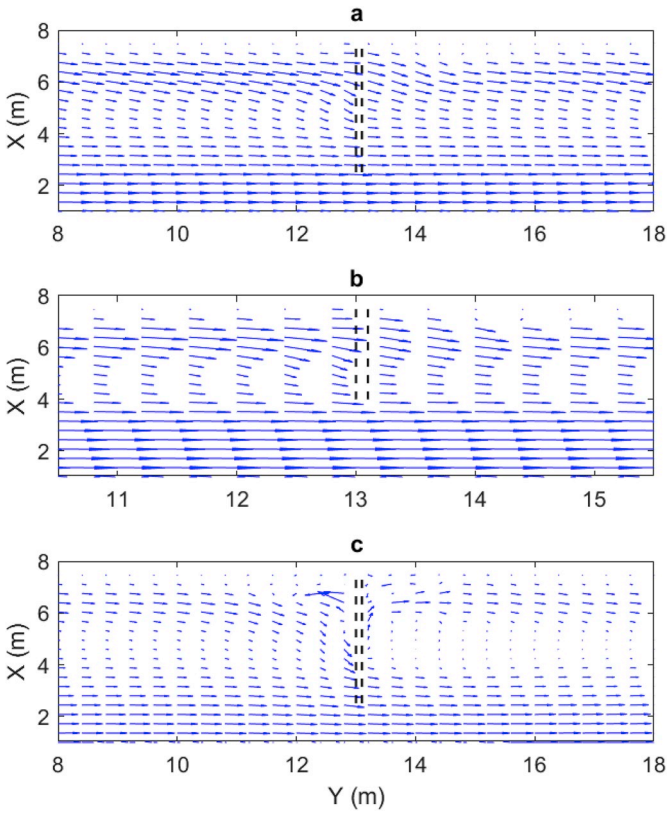

Fig. 22. The vector flow filed near the middle groin, within three long permeable groin field (a), five short permeable groin field (b), and three long impermeable groin field (c).

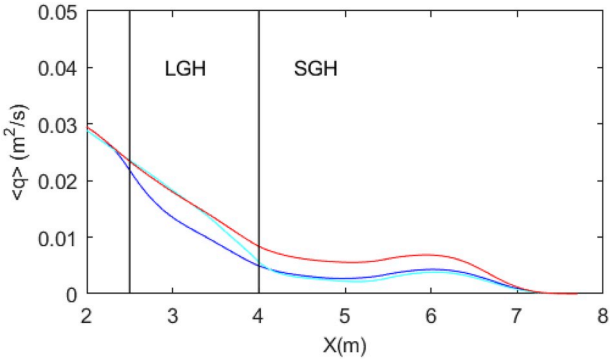

Fig. 23. The alongshore volume discharge <q> alongshore averaged in groin fields. (blue line: five-groin field, cyan line: three-groin field, red line: none-groin field, LGH: long groin head, SGH: short groin head). (For interpretation of the references to colour in this figure legend, the reader is referred to the Web version of this article.)

more efficiently at the outer seaward zone (from X = 2.5 m to X = 4 m). From the aspect of retardation extent of total longshore discharge integrated along groin length, the three-long groins are favorable to contribute to a larger retardation of total longshore discharge, although these two kinds of groin systems have a comparable total groin length.

5. Conclusion

The hydrodynamics of the flow within permeable pile groin fields on a beach slope was studied using the phase resolving wave-flow model SWASH. In this study, the multilayer mode of the SWASH model was validated to be able to predict longshore current profiles and groin-current interactions. Firstly, a uniform coast without groins was simulated to calibrate model parameters. The calculated longshore current distribution shows a good agreement with the laboratory observations (Hulsbergen and ter Horst, 1973). To validate the interactions between permeable pile groins and combined wave current flow, the pile groins were introduced in the calibrated model. These simulations clearly show that pile groins hardly attenuate the wave energy nearshore, the small wave height reduction was found only limited to wave shadow zone downdrift a groin. However, the longshore current velocities are retarded substantially by the pile groins. The retarded flow by pile groins are expected to weaken the ability to transport sediment alongshore. Within the groin fields, the retardation of longshore currents by a three groin system with a 55% permeability is up to 33% while a larger reduction degree of 43% is obtained within the groin embayment of a five groin system with a 50% permeability. An empirical formulation between the relative longshore current velocity and the groin permeability were given, which has a second order hyperbolic tangent form similar to that summarised by (Trampenau et al., 2004). The depth integration of longshore discharge suggests that long groins function more sufficiently compared with short groins, when their total lengths are comparable.

In addition to the variations of longshore currents at a groin engineered coast, the magnitudes of cross-shore currents were investigated too. The strong cross-shore currents are confined to breaker zone where the gradient of wave set up/down are large beside the groins. No obvious recirculation and eddies were found in both the three groin and five groin bays, due to their high permeability.

The overall consistence of the calculated results to the experimental measurements reveals a robust capacity of the SWASH model to calculate flow fields affected by permeable pile groins. Once the hydrodynamics of permeable pile groins are clear, longshore sediment transport could be predicted with more confidence. The deeper understandings we gained about the pile groin system by the use of numerical models, will in return benefit the design process of PPGs. Our future work would focus on the optimization of configuration parameters of PPGs and layouts of pile groin system.

Acknowledgements

This work is sponsored by the Chinese Scholarship Council (201406060020). We gratefully thank Dr. Hulsbergen for his explanations about the experimental apparatus, and Ir. De Wit, who extended the SWASH model for the application to include alongshore tidal currents. Finally, the detailed suggestions and advice from the reviewers are very appreciated which helped to improve this paper.

Appendix A

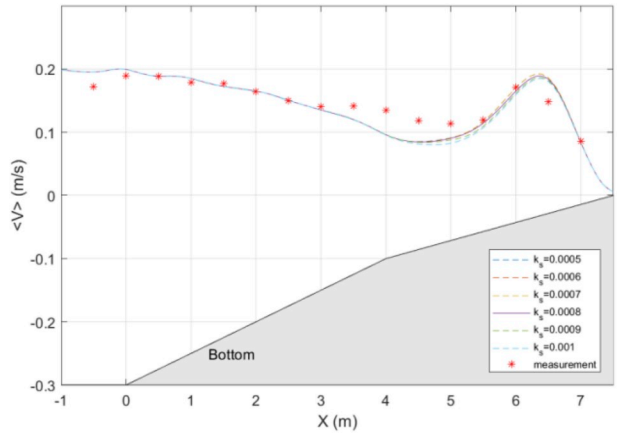

Fig. A1. The computed mean superfical longshore current velocities $< \overline{V_s} >$ with varying k_s coefficients under the combined wave-current condition.

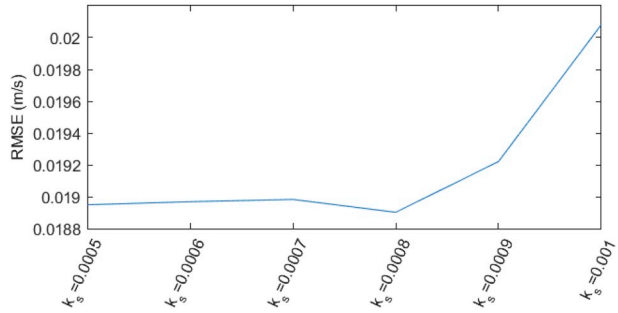

Fig. A2. The root mean square erros (RMSE) of computed mean superfical longshore current velocities $< \overline{V_s} >$ with varying ks coefficients against measurements.

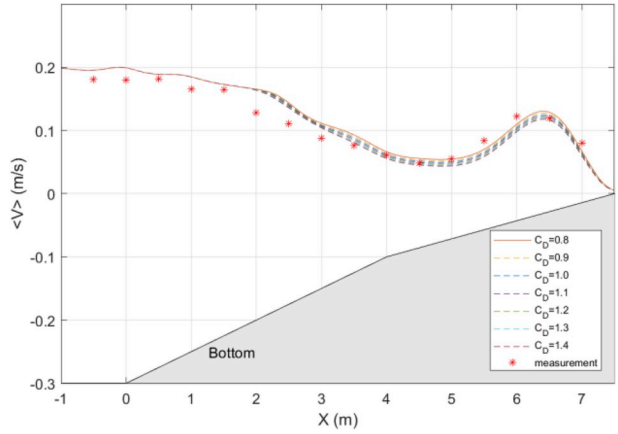

Fig. A3. The computed mean superfical longshore current velocities $< \overline{V_s} >$ alongshore averaged within three long groin field with varying C_D coefficients under the combined wave-current condition.3

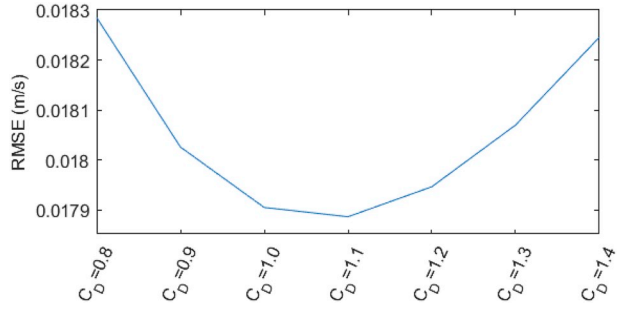

Fig. A4. The root mean square erros (RMSE) of computed mean superfical longshore current velocities $< \overline{V_s} >$ alongshore averaged within three long groin field with varying C_D coefficients against measurements.4

References

Abam, T.K.S., 2009. Bank erosion and protection in the Niger delta. Hydrol. Sci. J. 38, 231–241. https://doi.org/10.1080/02626669309492665.

Bakker, W.T., Hulsbergen, C.H., Roelse, P., de Smit, C., Svasek, J.N., 1984. Permeable groynes: experiments and practice in The Netherlands. In: 19th International Conference on Coastal Engineering, pp. 1983–1996. Houston.

Bakker, W.T., Klein Breteler, E.J.H., Roos, A., 1970. The dynamics of a coast with a groyne system. 12th Coast Eng. Conf. 1001–1020.

Crossman, M., 2004. Manual on the Use of Timber in Coastal and River Engineering. https://doi.org/10.1680/motuoticare.32835.

Crossman, M., Simm, J., 2002. Sustainable coastal defences - the use of timber and other materials. Proc. Inst. Civ. Eng. Munic. Eng. 151, 207–211. https://doi.org/10.1680/muen.151.3.207.38884.

De Wit, F., Tissier, M., Reniers, A., 2017. Including tidal currents in a wave-resolving model. Coast. Dyn. 1638–1648.

Dette, H.H., Raudkivi, A.J., Oumeraci, H., 2004. Permeable pile groin fields. J. Coast. Res. 145–159.

Hulsbergen, C.H., ter Horst, W., 1973. Effect of Permeable Pile Screens on Coastal Currents, vol. 1148. Delft Hydraulics laboratory report M, Delft (in Dutch).

Kolp, O., 1970. Farbsandversuche mit lumineszenten Sanden in Buhnenfeldern. Ein Beitrag zur Hydrographie der Ufernahen Meereszone. Petermanns Geogr. Mitt. 114 (2).

Launder, B.E., Spalding, D.B., 1974. The numerical computation of turbulent flows. Comput. Methods Appl. Mech. Eng. 3, 269–289. https://doi.org/10.1016/0045-7825(74)90029-2.

Nadaoka, K., Kondoh, T., 1982. Laboratory measurements of velocity field structure in the surf zone by LDV. Coast Eng. Jpn. 25, 125–145. https://doi.org/10.1080/05785634.1982.11924341.

Perdok, U., Crossman, Matt, Verhagen, H.J., Howard, S., Jonathan, S., 2003. Design of timber groynes. In: Coastal Structures, pp. 1689–1699. https://doi.org/10.1017/CBO9781107415324.004.

Perdok, U.H., 2002. Application of Timber Groynes (Technology).

Price, W.A., TOMLINSON, K.W., Willis, D.H., 1972. Filed tests on two permeable groynes. In: Coastal Engineering Proceedings, pp. 1312–1325. https://doi.org/10.1016/B978-0-7020-3935-5.00077-X.

Putrevu, U., Svendsen, I.A., 1993. Vertical structure of the undertow outside the surf zone. J. Geophys. Res. https://doi.org/10.1029/93JC02399.

Raudkivi, A.J., 1996. Permeable pile groins. J. Waterw. Port, Coast. Ocean Eng. 122, 267–272. https://doi.org/10.1061/(ASCE)0733-950X(1996)122:6(267).

Raudkivi, A.J., Dette, H.H., 2002. Reduction of sand demand for shore protection. Coast. Eng. 45, 239–259. https://doi.org/10.1016/S0378-3839(02)00036-4.

Rijnsdorp, D.P., Smit, P.B., Zijlema, M., Reniers, A.J.H.M., 2017. Efficient non-hydrostatic modelling of 3D wave-induced currents using a subgrid approach. Ocean Model. 116, 118–133. https://doi.org/10.1016/j.ocemod.2017.06.012.

Smagorinsky, J., 1963. General circulation experiments with the primitive equations. Mon. Weather Rev. 91, 99–164. https://doi.org/10.1175/1520-0493(1963)091<0099:GCEWTP>2.3.CO;2.

Smit, P., Zijlema, M., Stelling, G., 2013. Depth-induced wave breaking in a non-hydrostatic, near-shore wave model. Coast. Eng. 76, 1–16. https://doi.org/10.1016/J.COASTALENG.2013.01.008.

Strusiańska-Correia, A., 2014. Beach stabilization at Kołobrzeg, Poland. J. Coast. Res. 71, 131–142. https://doi.org/10.2112/SI71-016.1.

Trampenau, T., Goricke, F., Raudkivi, A.J., 1996. Permeable pile groins. In: 25th International Conference on Coastal Engineering, pp. 2142–2151. Orlando.

Trampenau, T., Oumeraci, H., Dette, H.H., 2004. Hydraulic functioning of permeable pile groins. J. Coast. Res. 160–187.

Uijttewaal, W.S., 2005. Effects of groyne layout on the flow in groyne fields: laboratory experiments. J. Hydraul. Eng. 131, 782–791. https://doi.org/10.1061/(ASCE)0733-9429(2005)131:9(782).

Zijlema, M., Stelling, G., Smit, P., 2011. SWASH: an operational public domain code for simulating wave fields and rapidly varied flows in coastal waters. Coast. Eng. 58, 992–1012. https://doi.org/10.1016/J.COASTALENG.2011.05.015.

Zijlema, M., Stelling, G.S., 2008. Efficient computation of surf zone waves using the nonlinear shallow water equations with non-hydrostatic pressure. Coast. Eng. 55, 780–790. https://doi.org/10.1016/J.COASTALENG.2008.02.020.

Zijlema, M., Stelling, G.S., 2005. Further experiences with computing non-hydrostatic free-surface flows involving water waves. Int. J. Numer. Methods Fluids 48, 169–197. https://doi.org/10.1002/fld.821.